PCCP

Accepted Manuscript

ROYAL SOCIETY OF CHEMISTRY

www.rsc.org/pccp

PCCP

ARTICLE

Water ingress into a casein film quantified using time-resolved neutron imaging

Received 00th January 20xx,
Accepted 00th January 20xx

DOI: 10.1039/x0xx00000x

www.rsc.org/

E. Metwalli[a], H.E. Hermes[b], E. Calzada[c], U. Kulozik[d], S.U. Egelhaaf[b] and P. Müller-Buschbaum[a]

The migration of water into a casein film was probed with neutron radiography. From the neutron transmission images, the evolution of the water saturation profiles was extracted. The results indicate that the water influx is dominated by imbibition but also contains a diffusional component. The time dependence of the water ingress was quantified using a diffusion-like equation previously also applied to imbibition. A water transport coefficient D = 0.9 x 10^{-9} m^2/s was found. This value and direct observation of the images indicate that the time taken for a typical adhesive casein-based layer to become saturated with water is of the order of hours.

1. Introduction

Casein proteins are a major component of milk. In aqueous solution they form casein micelles with a diameter of about 100 – 300 nm. Casein micelles are unique biocolloids of calcium, phosphate, and casein proteins. They not only play an important biological role in stabilizing the colloidal form of calcium phosphate in milk[1] but are also used in non-food applications such as adhesives, binders and protective coatings.[2, 3] Currently, aqueous mixtures of casein and alkaline materials such as lime are used to glue furniture, size canvas, and bind paint pigment. Furthermore, casein is widely employed as an adhesive for labeling glass bottles and other containers because casein-based adhesives provide superior mechanical stability over a broad range of humidities at temperatures between 2 and 40 °C.

The water molecules associated with the casein micelles are divided into different classes.[4] Usually, because of their strong association with the protein molecules, both the water molecules directly involved in the stabilization of the protein structure (structural water) and those which form a dynamically oriented monolayer with restricted motion (hydration water) are considered as bound water. By contrast, the hydrodynamic hydration water, which moves with the protein, while it is diffusing through the aqueous solution and which can exchange with the bound water, is referred to as "free" water. Various techniques have been applied to investigate the structure, mobility, extent, and modes of associated water molecules in different casein-based materials.[5-10]

Because casein proteins do not denature in the dry form, preparation of thin casein films similar to those used as adhesive films is possible.[11-14] These can be prepared by bulk or spin casting from aqueous solution. Metwalli *et al.*[15] investigated the time-evolution of water uptake by thin (1.42 μm thick) casein films in a water-vapor atmosphere using time-resolved grazing incidence small-angle neutron scattering (GISANS). The initially dry casein film, spin-coated onto silica, was exposed to water vapor at 30 °C. These thin films reached an equilibrated hydrated state after 11 min with a total content of 0.36 g water/g protein. Moreover, from this study information on the structural reorganization of casein micelles with respect to their size and size-distribution upon swelling after contact with water vapor was obtained. The size of the aggregates in a film depends not only on the size of the individual micelles but also on interactions between the micelles and with the casting surface as well as on subsequent treatment.[11]

In adhesive applications, films are used that are typically thicker than the 1-2 μm films required for GISANS and thus, water penetration on the macroscopic level is of prime interest. Hence, in the present investigation, we study the time-evolution of water migration into "thick" (hundreds of micrometers) casein films sandwiched between two parallel plates. The films have a cylindrical geometry with the top and bottom faces of the film covered and thus not accessible to water. This geometry and the larger thickness mimics casein-based adhesive films. Such films are mainly exposed to environmental moisture via their radial surfaces, for example, condensation water which forms when a bottle is removed from a cold storage and put to room temperature.

[a] *Technische Universität München, Physik-Department, Lehrstuhl für Funktionelle Materialien, James-Franck-Str.1, 85748 Garching, Germany Email: ezzmet@ph.tum.de, muellerb@ph.tum.de*
[b] *Condensed Matter Physics Laboratory, Heinrich Heine University, Universitätsstr. 1, 40225 Düsseldorf, Germany*
[c] *Technische Universität München, Heinz Maier-Leibnitz Zentrum (MLZ), Lichtenbergstr. 1, 85748 Garching, Germany*
[d] *Technische Universität München, Chair for Food Process Engineering and Dairy Technology, 85354 Freising-Weihenstephan, Germany*

Water transport into a film can occur by different mechanisms. When a dry or partially filled porous structure is contacted with a liquid, imbibition, diffusion or a combination of both may cause the liquid to enter the structure. During imbibition, capillary forces cause a wetting fluid, for example water, to be drawn into the structure where it replaces the non-wetting medium initially present, for example air or oil. By contrast, concentration gradients result in diffusion. When two materials are contacted, the concentration gradient leads to mixing. Although imbibition and diffusion are very different on a microscopic level, on larger length scales there are similarities. For example, in both transport mechanisms the interface between the two regions widens with time and a square-root-of-time dependence of the characteristic processes is often observed.[16-19] Frequently, similar mathematical relationships are found to apply to diffusion and imbibition (and, e.g., thermal conductivity) and their mathematical equivalence has been widely exploited.[16] For example, two-dimensional diffusional transport into an infinitely long cylinder with constant concentration at the radial surface was described by the appropriate diffusion equations. For a cylinder of radius a, the water saturation $S(r,t)$ as a function of radial position r, where r is measured from the radial surface of the cylinder, and time t is given by [17]

$$S(r,t) = 1 - 2\sum_{n=1}^{\infty} \frac{J_0\left(z_n \frac{(a-r)}{a}\right)}{z_n J_1(z_n)} e^{-\frac{D z_n^2}{a^2} t} \qquad (1)$$

where J_0 and J_1 are the Bessel functions of the first kind of zero and first order, respectively, z_n are the roots of $J_0(z_n) = 0$ and D is the transport coefficient, which we take to be independent of time. When calculating the sum, considering the first 40 terms (n = 1 … 40) is sufficient.[20] Through integration, the total water saturation $S_{tot}(t)$ of the cylinder can be obtained as

$$S_{tot}(t) = 1 - 4\sum_{n=1}^{\infty} \frac{1}{z_n^2} e^{-\frac{D z_n^2}{a^2} t} \qquad (2)$$

Hence, D can be obtained experimentally either through the water saturation profiles (**Equation 1**) or the total water saturation (**Equation 2**). Although based on the diffusion equation, these equations have been successfully applied to the imbibition of water into a cylindrical, initially oil-saturated porous material which has been brought in contact with pure water along its radial surface.[20]

Concentration or saturation profiles $S(r,t)$ can be obtained for a wide range of materials by neutron imaging. In principle, neutron imaging is a simple technique:[21] The sample is irradiated by an almost parallel beam of neutrons and the neutron transmission resolved spatially. If these measurements are quantitatively analyzed, the evolution of the local composition of the sample can be determined and converted into time-dependent saturation profiles.[21-23] Time-resolved neutron imaging has proved to be a valuable tool to study the migration of hydrogenous fluids (e.g. H_2O) into materials because of the strong neutron attenuation by the hydrogen nuclei.[24] For instance, neutron radiography was used to investigate water penetration and water distribution in geological samples and building materials.[25, 26] In addition, investigation of water transport in polymers[27] and polymer electrolyte fuel cells was successfully conducted with neutron radiography techniques.[28]

In the present investigation we focus on the use of neutron imaging to quantitatively investigate the ingress of water into casein films similar to those found in labeling applications. A better knowledge of the mechanisms and rates of moisture transport into adhesive films can improve our understanding of the impact of water on the mechanical stability and durability and, hence, the performance of adhesive films based on casein.

2. Materials and Methods

2.1 Sample

The casein micelles were prepared from skim milk using the microfiltration/ultrafiltration diafiltration process.[29] A gel consisting of 50 wt% casein micelles in heavy water (D_2O) was prepared and cast on one part of an aluminum cell.[23] After a few minutes, the cell was closed with the second part of the cell, which includes a spacer. The resulting film had a well-defined thickness of 0.3 mm. The thickness ensures sufficient beam attenuation for images of reasonable quality to be recorded during the exposure times. At the same time it allows formation of a well-defined macroscopically reasonably 'smooth' radial edge to result in a fairly sharp rise in the transmission. In the example discussed here, the radius of the resulting film was approximately 5.5 mm. In the sample cell, the disk-like film was initially surrounded by air. The casein film in the cell was heated to 50 °C for 30 min to dry the film and then kept at room temperature for 1 h before the neutron measurements were started and the film contacted with water (H_2O). Two small holes in opposite sides of the cell served as inlet and outlet for water.[23] During the measurements, the cell and hence the film was held vertically and temperature was recorded and found to be 26.5 ± 0.5 °C. A free-standing casein film could not be prepared because it was 'sticking' to the supporting solid surface.

2.2 Characterizations of the casein film

A dry casein film prepared in the cell was investigated using optical microscopy (OM), scanning electron microscopy (SEM), and atomic force microscopy (AFM) to study the multi-length scale porosity of the dry film. As the aluminum cell was opened, the film was cleaved into two parts attaching to the aluminum plates. OM images with magnification of 10x were collected for the film using a Zeiss Axiotech 25H optical microscope. SEM images were acquired using a Zeiss Gemini NVision 40 (5kW, 3.0 mm working distance, 10 μm aperture). An Autoprobe CP (Vecco) AFM was used for the investigation

of the casein film surfaces on the nanoscale. All measurements were performed under air and at room temperature. Although several images were taken, only one typical image from each technique is presented.

2.3 Time-resolved neutron imaging

The neutron imaging experiment was performed using the instrument ANTARES at the research reactor Forschungs-Neutronenquelle Heinz Maier-Leibnitz (MLZ) in Munich.[30] At the reactor's full power of 20 MW the neutron flux at the sample position is approximately 9 x 10^7 neutrons/cm^2/s for the chosen l/d = 400, where l is the collimator length and d the aperture diameter.[30] After penetrating the sample, the neutrons strike a scintillator plate that subsequently emits a cascade of photons. The light produced by the scintillator plate is directed by a mirror to a CCD camera with 2048 x 2048 pixels. With the set-up used, each pixel corresponds to 25 x 25 μm^2 in the sample plane. This is consistent with the spatial resolution given by the geometry of the instrument, $L/(l/d) \approx$ 50 µm, with a sample to scintillator distance L = 20 mm.

Neutron radiography images were collected over several hours with an acquisition time of 30 s per image. The individual measurement time represents a compromise between counting statistics and time resolution. For these experiments, 30 s is sufficiently short for the observed propagation speed of the front and the used spatial resolution to prevent image 'smearing'. While images were acquired, the film was contacted with light water (H_2O), which was introduced through the lower hole. The time t at which the casein film was completely surrounded by water was defined as t = 0 s.

To allow for a quantitative interpretation of the neutron images, the raw images, $I_{raw}(x,y)$, were corrected for background noise, using a "dark" image $I_d(x,y)$ obtained with all shutters closed, as well as for beam and detector inhomogeneities, using an "open beam" image $I_{ob}(x,y)$ obtained with the sample removed from the beam. Where appropriate, spurious data points, such as bright spots caused by gamma radiation, were omitted. Furthermore, the images were normalized using the intensity I_{ref} of a sample area of typically 30 x 30 pixels centered at (x_0,y_0), here representing pure water (H_2O), to obtain the transmission of the sample relative to the transmission of water[21]:

$$T^{(rel)}(x,y) = \frac{\frac{I_{raw}(x,y) - I_d(x,y)}{I_{ob}(x,y) - I_d(x,y)}}{\frac{I_{ref}(x_0,y_0) - I_d(x_0,y_0)}{I_{ob}(x_0,y_0) - I_d(x_0,y_0)}} \qquad (3)$$

Subsequently, transmission profiles $T^{(rel)}(r)$ were obtained by azimuthally averaging. Due to the rough and not perfectly circular shape of the casein film's rim, the averaging procedure can lead to a smoothening of the interface and hence some parts of the rim were disregarded. Finally, the relative transmission profile of the sample $T_s^{(rel)}(r,t)$ and the relative transmissions of the initial, $T_{ini}^{(rel)}$, and final, i.e. saturated, $T_{fin}^{(rel)}$, casein film can be used to determine the water saturation profile $S'(r,t)$ at intermediate times:

$$S'(r,t) = \frac{\ln T_s^{(rel)}(r,t) - \ln T_{ini}^{(rel)}}{\ln T_{fin}^{(rel)} - \ln T_{ini}^{(rel)}} \approx \frac{T_s^{(rel)}(r,t) - T_{ini}^{(rel)}}{T_{fin}^{(rel)} - T_{ini}^{(rel)}} \qquad (4)$$

During the finite measurement time, the film does not reach its final saturated state and hence $S(r,t)$ does not reach 1. To account for this, a coefficient α is introduced; $S(r,t) = S'(r,t)/\alpha$. The coefficient α is iteratively determined so that, using equation 2, a best-fit to the total water saturation $S_{tot}(t)$ at the end of the measurement is achieved.

The transmission depends exponentially on the sample composition, in this case the water saturation. However, for the high transmissions observed in this experiment a linear approximation is valid within experimental uncertainties. Furthermore, the attenuation by water (H_2O) is mainly due to incoherent scattering, which can severely affect the measured transmission, typically leading to an underestimated water content.[24, 31] Due to the very small thickness of the sample, these effects are negligible, as can be seen from the sharp image of the reservoir edge towards the sample cell and is expected from previous studies.[24, 31] In addition, this allows us to move the detector close to the sample (L = 20 mm) and hence obtain a better spatial resolution.

To account for the geometrical imperfections of the sample rim and the finite time required for water injection, we define r = 0 mm slightly inside the casein film, about 0.25 mm from the film-water interface. Thus, the effective radius of the film is a = 5.25 mm. At r = 0, the water saturation was set to $S(r = 0, t) = 1$. The lower limit of the water saturation is given by the initial saturation of the sample and defined as $S(0 < r \leq a, t = 0) = 0$. For the analysis approach used, the absolute water contents are not required. It would be possible to determine these if the experimental neutron attenuation coefficients of casein and water or casein content of the initial film would be known. However, these could not be determined independently because the values depend on the precise state of the film, which is sensitive to preparation details.

3. Results and discussion

The casein film structure is imaged on several length scales with optical microscopy (OM), atomic force microscopy (AFM) and scanning electron microscopy (SEM). Since the casein film is made up of casein micelles it shows a hierarchical porous structure with pores on a broad range of length scales (**Fig. 1).**

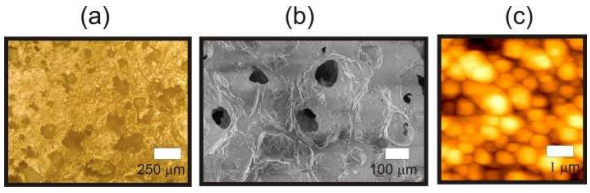

Fig. 1 (a) OM, (b) SEM, (c) AFM images of the casein film indicating the porous nature of the film at different length scales.

A typical series of neutron images obtained during water ingress into thick (hundreds of micrometers) casein films is shown in **Fig. 2**. In addition, to emphasize the water ingress into the casein film, a series of images divided by the image at t = 0 are shown in Fig. 3. Initially, the casein film is located in the center of the sample cell and surrounded by air (**Fig. 2a**). When the air is replaced by water (H_2O), the area surrounding the film appears darker because of the larger neutron attenuation of H_2O with respect to air (and D_2O) reduces the neutron transmission (**Fig. 2b**). Careful inspection of subsequent images reveals that the image of the casein film becomes darker, starting from the edge of the casein film and moving towards its center. This reflects the ingress of water into the sample (**Fig. 2c-f, 3a-f**). Initially, only the edge of the sample has darkened (0.5 h, **Fig. 2d, 3c**). Within 1 h, the transmission at the center of the sample has also been reduced (**Fig. 2e, 3d**). Throughout, the interface between the lighter and darker regions is poorly defined, suggesting a broad transition. After 1.5 h, the water saturation within the film appears to be almost homogeneous (**Fig. 2f, 3e**). During the whole process, no significant swelling of the film is observed.

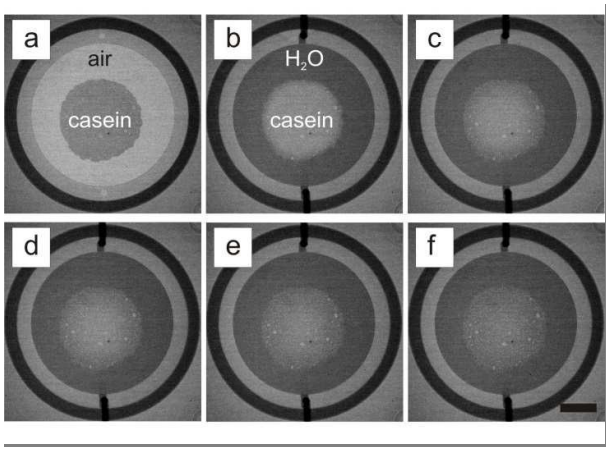

Fig. 2 Neutron transmission images during water migration into a 0.3 mm thick casein micelle film which is located in the center of an aluminum cell. (a) Initially the film is surrounded by air. (b-f) Water migration into the film at times t = 0, 1200, 1800, 3600, and 5400 s. The scale bar corresponds to 5 mm.

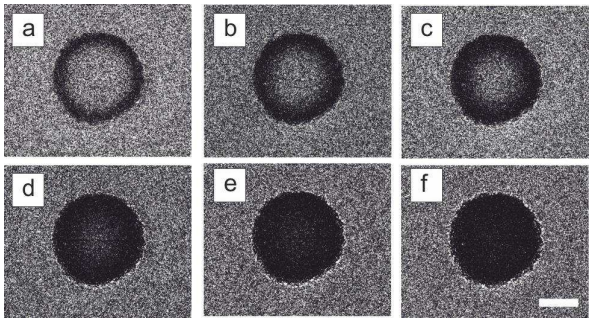

Fig. 3 Normalized neutron transmission images during water migration into a 0.3 mm thick casein micelle film at times t = 600, 1200, 1800, 3600, 5400 and 8010 s divided by the image at t = 0. The scale bar corresponds to 5 mm.

In addition to the water migration behavior, neutron radiography reveals large (≳ 100 μm), highly transparent areas in the casein film (**Fig. 2**). They become more obvious with time due to their increased contrast with the progressively H_2O-saturated casein. Their high transmission suggests that they represent trapped air or D_2O, i.e. they are macroscopic pockets in the casein film. As the pockets do not appear to move or change with time they are not expected to interfere with the water ingress. Apart from these pockets, the film appears homogenous. The slight graininess of the image is attributed to statistical fluctuations caused by the limited measurement time required to achieve the necessary time resolution in this kinetic study.

Profiles of the transmission normalized to H_2O, $T_s^{(rel)}(r,t)$, are extracted from the images for different elapsed times (**Fig. 4**). The transmission of the initial casein film ($T_s^{(rel)}(r,t=0)>1$) is higher than that of H_2O ($T_{H_2O}^{(rel)}=1$) and of pure casein. This is consistent with the presence of heavy water (D_2O) and air filled mesoscopic voids in the film. The transmission of the casein film decreases with time which corresponds to the darkening in the images and indicates an increase of the water (H_2O) content (**Fig. 2**). Water flux into the casein film continues for over an hour. This is much longer than the 11 min taken to attain saturation in the GISANS experiments [15] and is due to the different contact areas with respect to the volumes: In the GISANS experiments, the full top surface of a very short cylinder (top surface of a 1.42 μm thick film) was in contact with water (vapor), while in the present neutron imaging experiments, water enters only

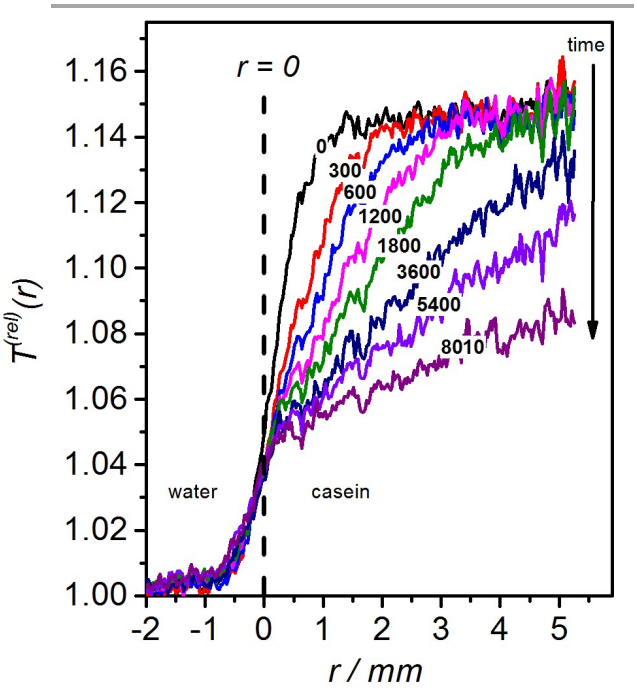

Fig. 4 Azimuthally averaged relative transmission profiles $T^{(rel)}(r)$ as a function of the distance from the rim of the film, r. They are calculated from the neutron images of the casein micelle film at different times after contact with water, t = 0, 300, 600, 1200, 1800, 3600, 5400, 8010 s (top to bottom).

through the radial surface of the cylinder, which in addition has a relatively large radius a = 5.25 mm.

Based on the transmission profiles, the water saturation profiles $S(r,t)$ are obtained (**Equation 4**). The profiles decay from the wet radial surface of the casein film, which was set to $S(r = 0, t) = 1$, to the center of the casein, which was initially set to $S(r = a, t = 0) = 0$ (Materials & Methods). The interface is seen to widen with time (**Fig. 5**). After approximately 0.5 h the water has reached the center of the film and after about 2.2 h the water saturation at the center has increased to about 0.65.

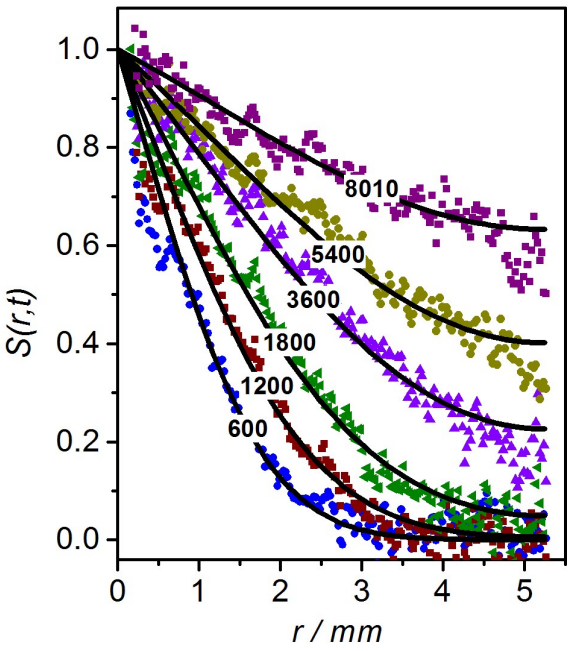

Fig. 5 Azimuthally averaged water saturation profile S(r,t) as a function of the distance from the rim of the film, r, at different times after contact with water, t = 600, 1200, 1800, 3600, 5400 s (bottom to top). The solid lines are fits based on

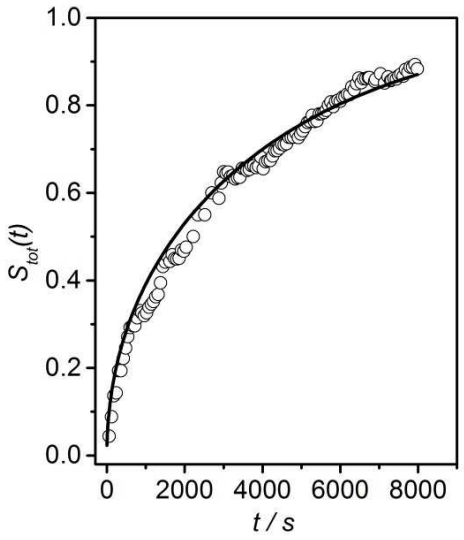

Fig. 6 Total water saturation $S_{tot}(t)$ of the casein micelle film as a function of time t after contact with water. The line is a fit based on equation 2.

The profiles provide more detailed and in particular quantitative information than the visual inspection of the images. For example, they reveal that at this time the water distribution is not yet homogeneous as is perhaps suggested by a visual examination of the image (**Fig. 2f**).

To quantify the increase in total water content, the amount of water in the whole film is determined as a function of time by summing the water saturation over the sample area (**Fig. 6**). After a fast initial increase in total water saturation $S_{tot}(t)$, a gradual saturation is observed at longer times. The time required to reach saturation depends on the size of the film (Eq. 2). Since adhesive labels are usually larger than the film investigated here, in practical applications the time required for the adhesive layer to approach complete water saturation is expected to be significantly longer than 2 h.

We now attempt a quantitative interpretation of the results in terms of imbibition and/or diffusion. If the initial film contained only bound water, the "dry" film represented a porous structure consisting of casein with its tightly bound water and air-filled voids. In this situation, water ingress proceeds through spontaneous imbibition and a transport coefficient D can be determined via either equation 1 or 2. In the other limiting case, i.e. if the film was initially completely saturated with water (D_2O) when contacted with light water (H_2O), diffusion would lead to an exchange between D_2O and H_2O. This diffusion process can also be described by equations 1 and 2 and a diffusion coefficient D can be obtained. These two scenarios represent the limiting cases. In any case, gravity can be neglected as the hydrostatic pressure is much lower than the capillary pressure in the small pores and gravity does also not affect the diffusion of water. From trial experiments, it is known that fully water saturated films of this geometry are unstable and flow under their own weight when placed in a vertical position. As a consequence, we exclude this limiting case from our considerations. On the other hand, due to the drying method (Materials & Methods), we do not expect to remove all the bulk water from the sample. Because the initial water content depends on sample preparation details, it cannot be determined from neutron images for these casein films (Materials & Methods). In our experiments, the initial

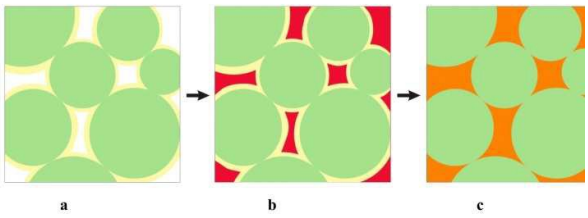

Fig. 7 (Color online) Schematic illustration of water ingress occurring via a combination of imbibition and diffusion. (a) Initially, voids [white] are present between the casein aggregates (with their bound water) [green] which are surrounded by a layer of "free" water (D_2O) [yellow]. In reality, the thickness of this layer is not necessarily homogenous and the aggregates not spherical. (b) Water (H2O) [red] imbibes into the voids in the sample and (c) mixes via diffusion with the layer of water (D2O) already present resulting in a homogeneous H_2O-D_2O mixture [orange] filling the voids.

film has been most likely partially saturated. In this intermediate situation, water (H_2O) is expected to flow into the voids (**Fig. 1**) by imbibition and simultaneously mix by diffusion with the D_2O initially present (**Fig. 7**). The diffusional exchange occurs on a microscopic length scale, of the order of the casein micelles (100 – 300 nm), and hence currently cannot be resolved by neutron imaging. Thus, although a combination of imbibition and diffusion is expected, it is anticipated that imbibition initially dominates and diffusion cannot be resolved. A partially saturated film will swell until osmotic pressure differences between it and the solvent are balanced. It may be expected that this effect will only be observed once the voids have been completely filled. Our experiments show that the casein film did not significantly change its size during the first about 1.5 h but that its edge then tended to soften and change shape slightly (**Fig. 2f**). This further suggests a combination of imbibition and diffusion processes.

By focusing on the mesoscopic rather than the microscopic level, both imbibition and diffusion can be described by the same equations (**Equations 1 and 2**). In the sample geometry used, the film had a cylindrical shape with its radial surface in contact with water while the top and bottom faces were inaccessible to water. Thus, equation 1 is fitted to the water saturation profiles $S(r, t)$ (**Fig. 5**). From equation 1 the fit of S(r,t) as a function of radius r provides time independent D values. The data appear to be well-described and a transport coefficient D could be extracted, $D = 0.92 (\pm 0.15) \times 10^{-9}$ m^2/s. Using the extracted D value in equation 2 enables a good fit to the total water saturation $S_{tot}(t)$ (**Fig. 6**) and yields a coefficient $\alpha = 1.075$, meaning that the film had reached about 93% of its full saturation state after the total measurement time of 8010 s.

In casein solutions and gels, it has been shown that the self-diffusion coefficient of water decreases with increasing casein concentration from 2.3×10^{-9} m^2/s for pure water to 1.4×10^{-9} m^2/s for solutions with 0.23 g casein/g water.[6] Our value is consistent with a higher casein content in the film. However, a quantitative comparison is not possible due to the different physical states considered, namely a 'dry' porous film and casein solutions, respectively. To our knowledge no values describing the mesoscopic transport of water in casein films are available in the literature.

Conclusions

Neutron imaging has been used to determine the time-evolution of the water saturation profile in a casein film after contact with water. The casein film was confined between two parallel plates, which rendered the faces of the film inaccessible to water so that water migration into the film only occurred via the small radial film surface. Thus, the film can be treated as an infinite cylinder. Our results suggest that water migration into the casein film can be quantitatively described by equations which have been applied not only to diffusion but also imbibition. A fit of these equations yielded a consistent water transport coefficient, $D \approx 0.9 \times 10^{-9}$ m^2/s. We expect imbibition to be the dominant mechanism of water ingress into casein films, but propose that diffusion between bulk water, the imbibed water and that already initially associated with the casein will also occur.

With respect to applications, such as paper labels glued to glass bottles, water ingress is a relatively slow process (hours), which is less critical since no long term stability is required. In contrast, in case of durable adhesive connections based on caseins, they will seriously suffer from water ingression. This can be retarded by inclusion of additives.

Acknowledgements

We thank the Heinrich-Heine University Düsseldorf for partial funding via their Strategic Research Fund, the Nanosystems Initiative Munich (NIM) and the Deutsche Forschungsgemeinschaft (grant number MU1487/6) for financial support. The neutron source Heinz Maier-Leibnitz (MLZ) is acknowledged for providing beam time. We are grateful to Patrick Huber for helpful discussions.

References

1. C. Holt, in *In Developments in Dairy Chemistry-3*, ed. P. F. Fox, Elsevier Applied Science Publishers, London, 1985.
2. J. L. Audic, B. Chaufer and G. Daufin, *Lait*, 2003, **83**, 417-438.
3. C. R. Southward and N. J. Walker, *New Zeal J Dairy Sci*, 1980, **15**, 201-217.
4. J. E. Kinsella and P. F. Fox, *Crc Cr Rev Food Sci*, 1986, **24**, 91-139.
5. A. Anagnostopouloukonsta and P. Pissis, *J Phys D Appl Phys*, 1987, **20**, 1168-1174.
6. F. Mariette, D. Topgaard, B. Jonsson and O. Soderman, *J Agr Food Chem*, 2002, **50**, 4295-4302.
7. M. T. Kalichevsky and J. M. V. Blanshard, *Carbohyd Polym*, 1992, **19**, 271-278.
8. T. F. Kumosinski, G. King and H. M. Farrell, *J Protein Chem*, 1994, **13**, 701-714.
9. R. Gebhardt and U. Kulozik, *Food Funct*, 2014, **5**, 780-785.
10. R. Gebhardt, *J Appl Crystallogr*, 2014, **47**, 29-34.
11. P. Müller-Buschbaum, R. Gebhardt, E. Maurer, E. Bauer, R. Gehrke and W. Doster, *Biomacromolecules*, 2006, **7**, 1773-1780.
12. P. Müller-Buschbaum, R. Gebhardt, S. V. Roth, E. Metwalli and W. Doster, *Biophys J*, 2007, **93**, 960-968.
13. R. Gebhardt, S. V. Roth, M. Burghammer, C. Riekel, A. Tolkach, U. Kulozik and P. Müller-Buschbaum, *Int Dairy J*, 2010, **20**, 203-211.
14. R. Gebhardt, M. Burghammer, C. Riekel, U. Kulozik and P. Muller-Buschbaum, *Dairy Sci Technol*, 2010, **90**, 75-86.
15. E. Metwalli, J. F. Moulin, R. Gebhardt, R. Cubitt, A. Tolkach, U. Kulozik and P. Müller-Buschbaum, *Langmuir*, 2009, **25**, 4124-4131.
16. M. Sahimi, *Flow and Transport in Porous Media and Fractured Rock*, Wiley.VCH, 2nd edn., 2011.
17. J. Crank, *The Mathematics of Diffusion*, Oxford University Press, Oxford, 1975.

18. M. Reyssat, L. Courbin, E. Reyssat and H. A. Stone, *J Fluid Mech*, 2008, **615**, 335-344.
19. M. Alava, M. Dube and M. Rost, *Adv Phys*, 2004, **53**, 83-175.
20. D. C. Standnes, *J Petrol Sci Eng*, 2006, **50**, 151-160.
21. D. Wagner, M. Börgardts, C. Grünzweig, E. Lehmann, T. J. J. Müller, S. U. Egelhaaf and H. E. Hermes, *Rev Sci Instrum*, 2015, **86**, 093706
22. S. Gruener, Z. Sadjadi, H. E. Hermes, A. V. Kityk, K. Knorr, S. U. Egelhaaf, H. Rieger and P. Huber, *P Natl Acad Sci USA*, 2012, **109**, 10245-10250.
23. H. E. Hermes, C. E. Sitta, B. Schillinger, H. Lowen and S. U. Egelhaaf, *Phys Chem Chem Phys*, 2015, **17**, 15781-15787.
24. E. H. Lehmann, P. Vontobel and N. Kardjilov, *Appl Radiat Isotopes*, 2004, **61**, 503-509.
25. J. J. Milczarek, A. Czachor, A. E. El Abd and Z. Wisniewski, *Nucl Instrum Meth A*, 2005, **542**, 232-236.
26. A. Nordlund, P. Linden, G. Por, M. Solymar and B. Dahl, *Nucl Instrum Meth A*, 2001, **462**, 457-462.
27. J. T. Lindsay, M. Matsubayashi and M. N. Islam, *Nucl Instrum Meth A*, 1994, **353**, 149-151.
28. K. T. Cho, A. Turhan, J. H. Lee, J. S. Brenizer, A. K. Heller, L. Shi and M. M. Mench, *Nucl Instrum Meth A*, 2009, **605**, 119-122.
29. M. P. Bonisch, T. C. Heidebach and U. Kulozik, *Food Hydrocolloid*, 2008, **22**, 288-297.
30. B. Schillinger, E. Calzada, F. Grunauer and E. Steichele, *Appl Radiat Isotopes*, 2004, **61**, 653-657.
31. M. Kang, H. Z. Bilheux, S. Voisin, C. L. Cheng, E. Perfect, J. Horita and J. M. Warren, *Nucl Instrum Meth A*, 2013, **708**, 24-31.